RSC Advances

PAPER

View Article Online
View Journal | View Issue

Cite this: *RSC Adv.*, 2022, **12**, 31264

Aqueous/non-aqueous electrolyte tradeoffs in charge transfer and electrochromics of pseudocapacitive oxide films

Tinsley Elizabeth Benhaddouch, Shekhar Bhansali and Dongmei Dong *

Environmental sustainability, safety, cost, and performance are the driving metrics for modern technological developments. Progress in these realms has been made for electrochromic (EC) devices by optimizing anode/cathode electrode materials. Yet, by these standards, the role of the electrolyte has remained unexplored. This investigation on charge transfer mechanisms at the electrolyte/electrode interface facilitates a contrast of the aqueous and non-aqueous electrolytes studied. A classic EC, high-performing, non-aqueous, lithium chlorine oxide in propylene carbonate (PC-$LiClO_4$) is examined against a non-flammable, low reactive, cost-effective, aqueous, potassium hydroxide (KOH) electrolyte; to strengthen the understanding of electrochromics the electrolytes are referenced against the anodic EC nickel oxide (NiO) thin films. The KOH presents as a diffusion dominant response, supported by the findings of the cyclic voltammetry and electrochemistry impedance data ($b = 0.56$, 45°∠), respectively, compared to the more surface capacitive PC-$LiClO_4$ ($b = 0.68$, 60°∠). Interestingly, despite the KOH full redox potential window being half the PC-$LiClO_4$, the KOH system's current density reached more than 3 times higher than PC-$LiClO_4$. Additionally, realizing the same current density (2 mA cm^{-2}) in multi-step chronoamperometry, the required potential is ~5 times lower for KOH than for PC-$LiClO_4$ electrolyte, albeit the KOH has a longer response time. Inherent tradeoffs in the systems are considered for theoretical analysis of these phenomena, *i.e.*, molar mass, ionization energy, viscosity, *etc.* The chemical nature of the electrolyte shows a profound effect on electrochemical kinetics at the NiO/electrolyte interface, pointing to the significance of all aspects in an electrochemical cell. The coupled effect of the electrolyte composition/electrode material pairing dictates the charge-storage mechanisms (and subsequently, EC properties). Furthermore, knowledge of contrasts in electrolyte type is of great interest to the scientific community for the modern metric-based optimizations of many other clean energy systems.

Received 16th September 2022
Accepted 24th October 2022

DOI: 10.1039/d2ra05851k

rsc.li/rsc-advances

Introduction

Electrochromic (EC) devices have promising applications such as modern windows for enhanced climate control[1] by reducing A/C use supporting energy-waste reduction and glare-free rear-view mirrors for better night vision and road safety.[2] The coupled optical modulation and charge storage capacity could even be leveraged for energy storage devices with a visualized state of charge.[3] For any of these applications, a key concern among the many design metrics is reducing the unit cost while retaining performance and environmental sustainability. To design according to these metrics, we must carefully consider every individual component of the device.

The full device is a sandwich structure: substrate/conductor/anodic-thin-film/electrolyte/cathodic thin film/conductor. Transparent substrates such as glass or PET (polyethylene terephthalate) are important to allow the visibility of the optical properties of the EC films. Likewise, the transparency of the conductive layer is just as critical so ITO (indium tin oxide) or FTO (fluoride tin oxide) are suitable for this layer (although a more flexible alternative would be beneficial to the scientific community). To achieve optimal EC optics a cathodic thin film such as tungsten oxide (WO_3) needs to be paired with an anodic thin film such as nickel oxide (NiO). This is because the cathodic thin films color under charge insertion, and the anodic thin films color under charge extraction. Therefore, both sides will color simultaneously, therefore the entire device will be in a uniform state (colored or bleached). Most of the current research on EC oxides is limited to cathodic WO_3; however, the EC mechanisms in anodic NiO remain less explored and are unclear at present, especially the interaction between ionic species in electrolytes and electrodes, which points a direction to this study. To decouple the contributions of the anodic thin films from the full device structure we carried out this investigation in the half-cell configuration: substrate/conductive layer/

Department of Electrical and Computer Engineering, Florida International University, Miami, Florida, USA. E-mail: ddong@fiu.edu

anodic thin film in the electrolytes of interest. Considering the design metrics, NiO is an optimal anodic film because of its elemental abundance on earth[4] and ultra-low cost[5] compared to other anodic films, *e.g.*, iridium oxide[6] or cobalt oxide.[7]

The challenge of nickel oxide is its large optical modulation and high cycle life. To date, such studies focus on electrode materials; for example, electrodes have been optimized by material selection, nanostructuring,[8] doping to tune the work functions,[9] novel fabrication methods,[10] or device configurations.[11] It has been stated that the structural properties is related to the functional (electrochromic, electrical, durability) of the films.[12] Yet, when considering all the components in either a full-cell or half-cell configuration, the electrolyte is clearly essential and must also play a role in these functional properties of the system. Since the discovery of the first EC device by Deb[13,14] in 1969, various electrolytes have been tested for EC compatibility as outlined by Ding *et al.*[15] in the comprehensive review. Although recent interest is geared toward polymerized electrolytes, modern methods exist to transform traditional liquid electrolytes into suitable quasi-solid gel polymer electrolytes. The comparison of the liquid *vs.* gel versions of the same electrolytes demonstrates a comparable performance in cyclic voltammetry with an increase in cycle stability for the gel version.[16] Therefore, investigating the performance and charge storage mechanisms of liquid electrolytes is still relevant and insightful toward the fundamental understanding of the electrolytes and ultimately device commercialization. We acknowledge the pioneering work of Chen *et al.*, who studied electrolyte properties *via* the concentrations and doping ratios (*e.g.*, to improve the solubility of salts in organic solvents).[17] And of the work by Stenman whose work investigated electrolytes as a function of anion and cation for the optical transmittance, absorbance, color efficiency, and cycling stability.[18] To supplement their efforts, this work takes a focal consideration on electrolytes: that a switch in electrolytes would effectively change the electrochemical kinetics and overall response of electrochemical systems.

The creativity of this work lies in setting the spotlight on the electrolyte's role in the charge transfer process. To approach the critical challenge of optimizing the EC system for both optical modulation and cyclability, efforts are made to distinguish the charge transfer characteristics in two specially selected electrolytes with different working mechanisms and different functional properties. On this premise and expanding upon the work of those before, we select the lithium-based electrolyte PC-$LiClO_4$ selected for great compatibility with both NiO and WO_3 electrodes[19] and the protonic-based electrolyte KOH (selected for demonstrating the broadest optical modulation, charge storage, and cycle durability for NiO films). A second major challenge with full-device compatibility is that some of the most anodically compatible electrolytes such as KOH show little compatibility to cathodic electrodes.[20] Therefore, understanding the charge storage mechanisms in high-performing NiO-compatible electrolytes can then be used to tailor electrolytes that will also be compatible with the WO_3 electrode, while still maintaining optimal anodic performance functionalities.

As we theorize which additional features of the electrolyte impact the functional properties of the system, we employ the concept of tradeoff theory (common in the engineering disciplines). There are always tradeoffs, *i.e.*, compromises made to optimize the system for a certain perceived benefit: cost, environmental considerations, performance, durability, and bio-interfacing, to name a few. To determine the ideal electrolyte optimal for ionic conductivity and electrochromism (*i.e.*, optimized for performance), we consider tradeoffs within the electrolyte. For instance, Xu *et al.*[21] stated that good ion conductivity should result from a compromise between a high degree of dissociation and low mobility. Another tradeoff reported by Chen *et al.*[22] is between a high quantity of free ions and the mobility of ionic carriers. This work investigates the effect of water-based and organic solutions with the selected aqueous KOH and non-aqueous PC-$LiClO_4$ with a tradeoff concept, with consideration of the role the ions (OH^-, Li^+) play in the electrochemical systems. Comparing the KOH to $LiClO_4$, their ionization energy, and electron affinity will affect the dissociation, and the molar mass will make a difference in the mobility of the ion carriers in the electrolyte. The viscosity of the aqueous *vs.* non-aqueous electrolytes also changes ion mobility. The coupling effect of the electrolyte composition and electrode materials determines the charge-storage mechanism and EC properties and is not negligible for accomplishing extraordinary electrochemical performance for most other clean energy systems (fuel cells, solar cells, electrolyzers, *etc.*).

Results and discussion

Electrochromic properties

The EC optical properties of the NiO thin films are as demonstrated in Fig. 1. The EC NiO is capable of changing color within the visible spectrum, observable to the naked eye. The change in optical transmittance is a response to the positively and negatively applied voltages in the three-electrode system and the subsequent Li insertion/extraction (Fig. 1a). These optical changes can function as a visible representation of the energy storage/release, for example, we can observe the "partially colored" colored region in Fig. 1a is less intense comparing to the fully saturated state. The colored state in Fig. 1a is partially colored because the voltage applied is less than the voltage applied to achieve the "fully" colored state. This is further demonstrated in Fig. 8a. Extending beyond the qualification from visible observations we quantify these observations *via* optical transmittance spectra as shown in Fig. 1c. The NiO film does not approach 100% transmittance; the highest transmittance reached is approximately 80% around the 600 and 950 nm wavelengths for the most bleached state at −0.5 V potential. Additionally, for the most colored state at the +1.2 V potential, the transmittance trends up from about 15% to 35% in the visible spectra and continues to higher transmittance approaching the 1000 nm wavelength. Another observation is the repeatability of the response from the positive applied voltage for the most colored state shown in the nearly overlapping lowest transmission lines represented by the yellow and pink curves on the graph. This repeatability demonstrates

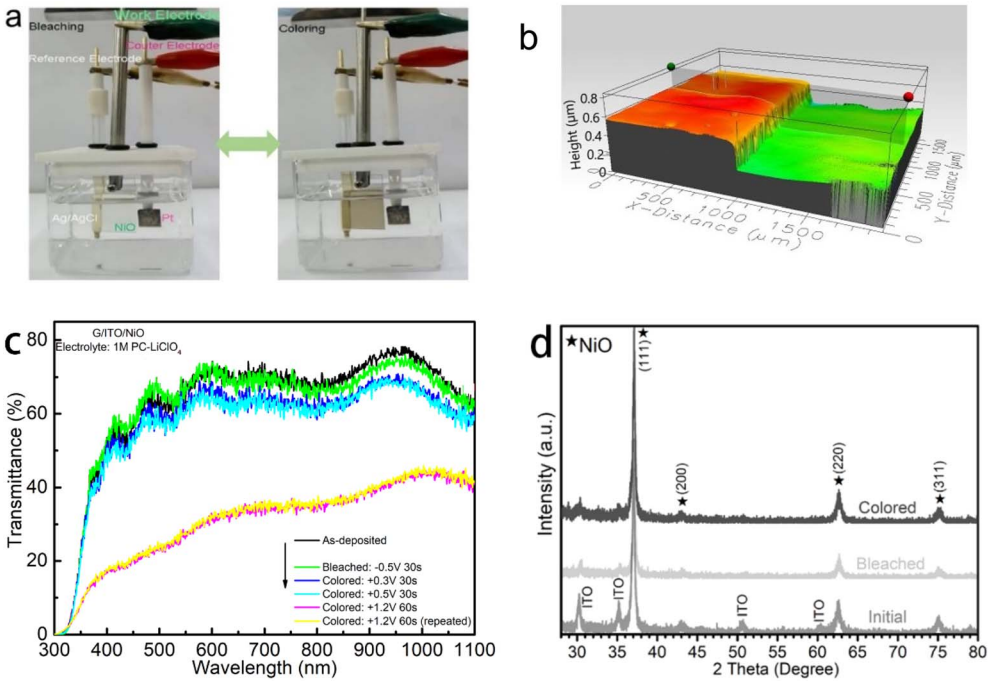

Fig. 1 (a) Electrochemical test setup; (b) surface imaging; (c) optical modulation of NiO thin solid film as deposited, in the bleached state and colored states; and (d) XRD patterns of initial/colored/bleached states.

stability which is promising for NiO and is consistent with the theory of the repeatability of the second of the two-stage processes proposed by S. Passerini and B. Scrosati.[23] Once the NiO is activated, the Li insertion into the NiO is easier to repeat. This is because there is a strong initial activation energy for the EC properties of the NiO film in this PC-$LiClO_4$ electrolyte as described by Wen *et al.*[20] in their comparison of the inserted charge *vs.* the extracted charge as a function of cycle.

Surface imaging and the EC NiO film thickness of ~350 nm are shown in Fig. 1b. X-ray Diffraction (XRD) has been carried out to investigate the structural changes of the thin film in the EC process (Fig. 1d). We see the regions of preferential NiO growth in the (111) planar direction. Compared to the initial state in the XRD image, there appears to be no significant changes in the overall structure as it switches to the colored or bleached states. Additionally, we see a very slight peak shift right in the (111) planar direction in bleaching but shifts back left in the colored state. These slight, reversible changes could be indicative of the ion insertion-induced stress in NiO films.

Distinct charging mechanisms for aqueous/non-aqueous environments

Cyclic voltammetry. Benefiting from electrochemical cycling of NiO in alkaline media has been studied for a while, initially in the scope of electrical batteries and then for electrochromics, the electrochemical reaction schemes have been established, generally, as follows:[24] $NiO + 2KOH \rightarrow Ni(OH)_2 + K_2O$; $Ni(OH)_2$ (bleached) + $OH^- \leftrightarrow$ NiOOH (colored) + $H_2O + e^-$; in comparison, in Li^+-containing electrolytes, $NiO_x + yLi^+ + ye^- \rightarrow Li_yNiO_x$; Li_yNiO_x (bleached) $\leftrightarrow Li_{y-z}NiO_x$ (colored) + $zLi^+ + ze^-$.

To comprehensively study the pseudocapacitive charge storage of the NiO film as well as the electrochemical kinetics,

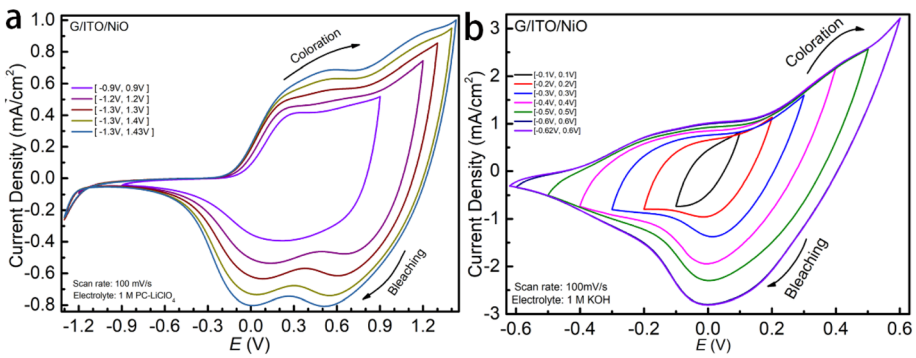

Fig. 2 (a and b) CV of NiO in 1 M $LiClO_4$-PC and 1 M KOH as a function of potential windows.

we start the cyclic voltammetry (CV) cycling of NiO in 1 M $LiClO_4$-PC at smaller potential windows and increase it until the redox peaks are complete for NiO, as shown in Fig. 2a. At the narrow potential windows, a peak centered around +0.3 V relates to the coloration. As the potential windows expand, this peak broadens and shifts towards the right, settling at +0.5 V. Initially, no peaks corresponding to the bleaching process show up in the smaller potential window; however, at the optimal potential window, two distinct peaks are observed around +0.5 V and 0 V. These peaks are broader at smaller potential windows and become narrower and more distinct as the potential window expands. Fig. 2b shows NiO films' electrochemical properties that allow easy comparison between 1 M KOH and 1 M $LiClO_4$. The shape of the CV curves indicates that the electrochemistry for the charge insertion/extraction is different in Li-PC and KOH. As a result, the charge capacity, represented by the area cycled by the CV curve is significantly higher in KOH aqueous electrolyte. The overall shape of NiO in both of the two electrolytes corresponds to typical pseudocapacitive behaviors with broad oxidation and reduction features appearing. However, a multi-step electrochemical process in the Li-PC is reflected by more than one redox peak. Due to the fast electrochemical response, the parameters of the CV experiments were run at relatively fast scan rates, Fig. 3a and c starting from 200 to 50 mV s^{-1}. We observe the highest current densities below +1.5 mA cm^{-2} in the potential window [−1.2 V, +1.3 V]. Interestingly, we see a vastly different response of NiO in the 1 M KOH. The optimal potential window allowing the full intercalation/de-intercalation is much narrower at a potential window of [−0.45, +0.45 V], whereas for 1 M $LiClO_4$-PC the potential window is up to [−1.2 V, +1.3 V]. The KOH results in much higher current densities (about 1.2 mA cm^{-2} and 3.5 mA cm^{-2}) compared to the NiO in the $LiClO_4$-PC with a current density of 1.0 mA cm^{-2} and 1.5 mA cm^{-2}. As you can see the KOH electrolyte is reaching nearly twice the peak current density as the Li-electrolyte with half of the applied potential window. There is no need to increase the potential window for the KOH any further for this study. This effect is explained by the ion insertion mechanism of the electrolytes (which will be discussed in further detail).

Multiple scan rates CV have been conducted to reveal the charge transfer kinetics, as shown in Fig. 3a and c. To quantitively distinguish the faradaic and capacitive behavior of the NiO in the two electrolytes, we employ the $\log i_P$ *vs.* $\log v$ analysis[25] as plotted in Fig. 3b and d for the $LiClO_4$-PC and KOH, respectively. v is the scan rate, and a and b are interchangeable values. To interpret these data sets, $b = 1.0$ corresponds to a capacitive-like, surface-dominant response, whereas $b = 0.5$ is a diffusion-controlled response. Applying this, we confirm that the fitted b values of NiO in the $LiClO_4$-PC, being about $b = 0.68$, demonstrate a diffusion-dominant and capacitive-like behavior through the processes. Comparatively, the nickel oxide in KOH has a fitted b value at approximately $b = 0.56$, which denotes a significantly more diffusion-controlled process with the slightest deviance towards a capacitive-like response. $\log i_P = b \times \log v + \log a$. The surface-redox and insertion (bulk) kinetics

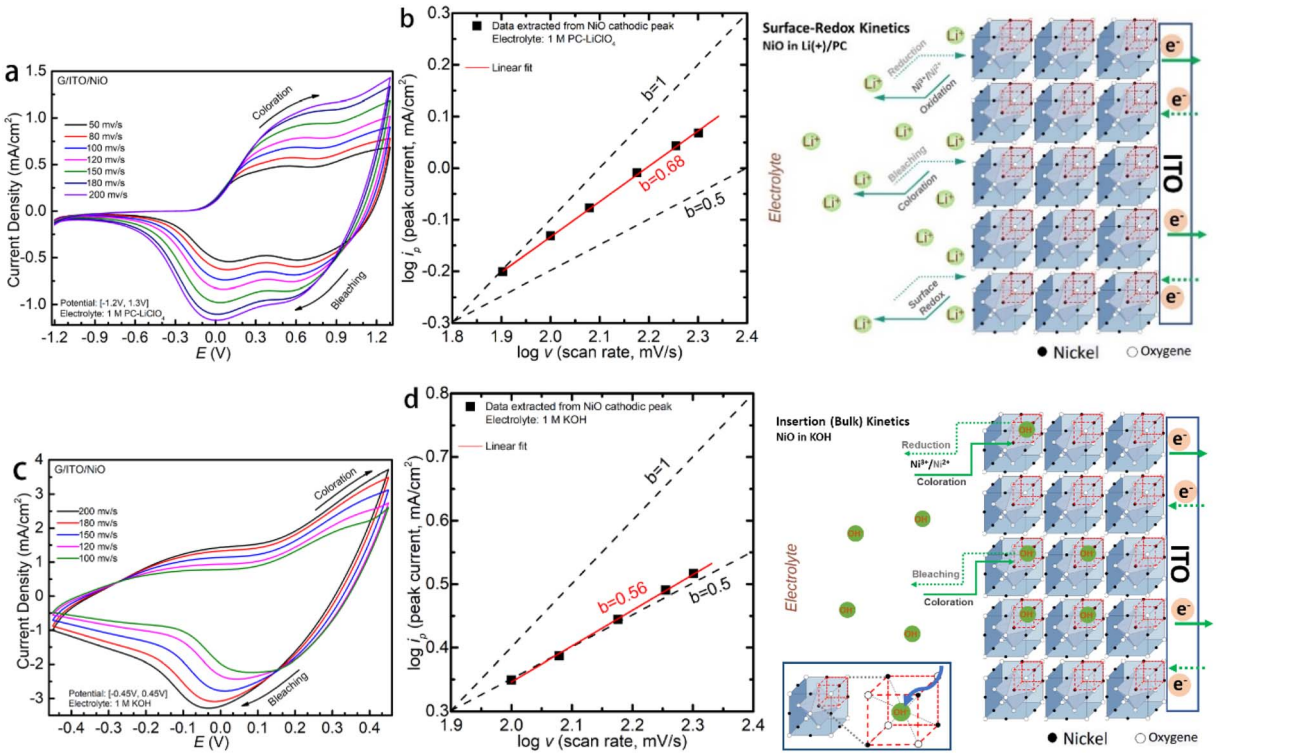

Fig. 3 (a and c) CV curves at different scan rates of NiO in Li-PC and KOH, respectively; (b and d) linear fitting of $\log i_P$ *vs.* $\log v$ and proposed dominant electrochemical kinetics at the interface in Li-PC and KOH, respectively.

mechanism are proposed for NiO in non-aqueous Li-PC and aqueous KOH electrolytes. Correspondingly, the mechanisms are also proposed for Li-PC and KOH, respectively. For the functional cations Li^+, the surface capacitive redox is dominant, while it is ion-insertion (bulk) into the NiO face-center-cubic as dominant kinetics for the functional anions OH^-.

Multi-step chronoamperometry (MSCA). In addition to CV, a constant potential is applied with different magnitudes and duration times (Fig. 4). As denoted for the anodic EC NiO film, the upper curves of the current density response correspond to the coloration, while the lower corresponds with bleaching. Another feature of NiO response present in both electrolytes is the current density approaching zero for both the Li^+ insertion and extraction processes, which differs from the cathodic WO_3.[26] In the PC-$LiClO_4$ electrolyte, we modulated the applied potentials from $\pm$0.3 V through $\pm$1.0 V; the duration of potential hold is 30 s for the first set and 60 s for the second set. Even though the applied potentials are different for each electrolyte you can see that both electrolytes are reaching comparable peak current densities, approximately 2 mA cm^{-2} for the highest applied voltage. This allows for comparability between the electrolytes without the system being influenced by the effect of potential. Observation is of slight asymmetry. Comparing a positively applied voltage against its reverse in equal magnitude, we see the current response shows a slight asymmetry indicating a not fully reversible reaction. Examining the multi-step chronoamperometry (MSCA) results of NiO in KOH, we modulated the applied potentials from $\pm$0.1 V through $\pm$0.2 V; the duration of potential hold is 30 s for the first set and 60 s for the second set. What differs between the electrolytes is that there are slightly broader, *i.e.*, less sharp peaks in the KOH electrolyte. This broadness in current density change indicates a slower response time. It is consistent with the results derived from the log i_P *vs.* log v plot of NiO in KOH being more diffusion-dominant relative to the PC-$LiClO_4$. Especially significant to note is that the current density in the KOH can reach a peak current density of 2 mA cm^{-2} at a small driving potential of 0.2 V, whereas to reach the same peak current density of 2 mA cm^{-2} using the PC-$LiClO_4$ required a 5 times higher potential of 1.0 V. It is noteworthy that the response differs between the two electrolytes, consistent with the 3D Bode plot results. In KOH, the response for coloration and bleaching is more equal, while it is much faster in bleaching in Li-PC. This is also a very interesting part of the study which speaks again toward the diffusion dominant *vs.* capacitive dominant response, dependent on the electrolyte. With the KOH we see that the coloration process and the bleaching process are more symmetrical to each other and overall, both slower than the Li-PC electrolyte. This corresponds to the diffusion-controlled kinetics for charge insertion and extraction. On the other hand, the Li-PC

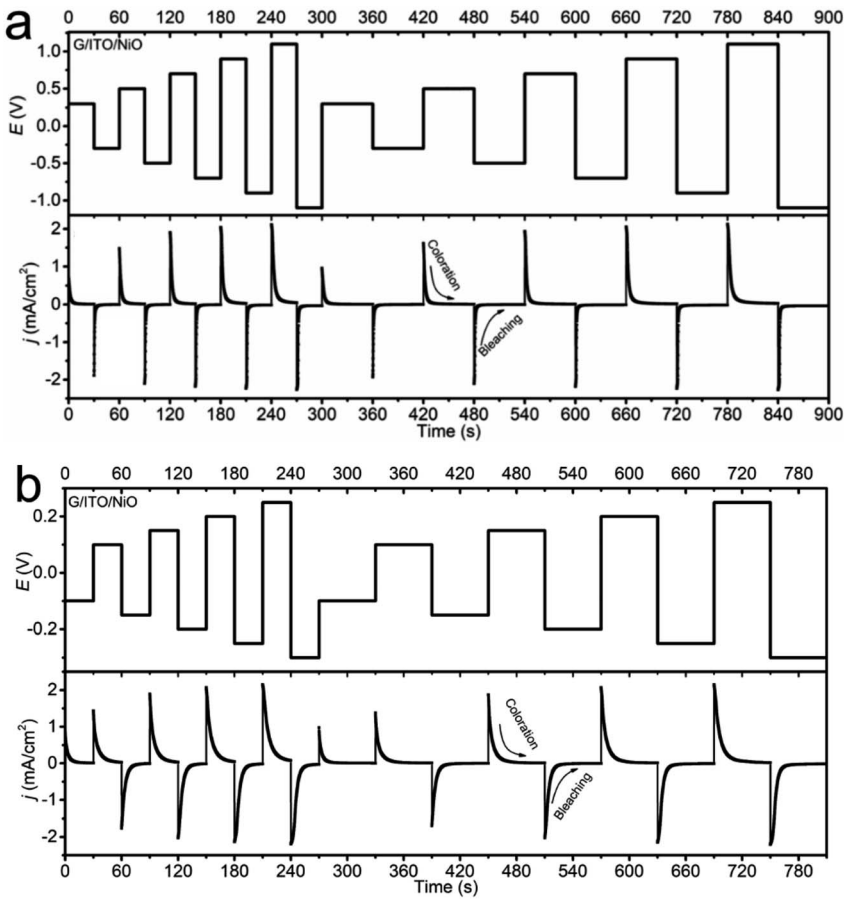

Fig. 4 MSCA response of NiO in (a) 1 M PC-$LiClO_4$ and (b) in 1 M KOH.

coloration is surface capacitive dominant, comparable to a true capacitor. Therefore, as the PC-Li demonstrates the pseudocapacitive response we expect a very fast bleaching process, again comparable to the fast discharge rate of a capacitor. The response of pseudocapacitive systems *vs.* diffusion-controlled systems correspond well with literature. Shao *et al.* investigates a pseudocapacitive film where a fast response time is evident[27] and Klymenko *et al.*[28] investigates a diffusion dominant system where we see the symmetry and slower response times This is quite interesting, and more insights are obtained from the impedance studies in the subsequent section.

Electrochemistry impedance spectroscopy (EIS)

Nyquist plot and model. The investigation of electrochemistry impedance spectroscopy (EIS) for the frequency response is of great interest for characterizing thin film super capacitance and charge transfer resistance features. EIS can assist in distinguishing between diffusion or pseudocapacitive mechanisms and identify which is more dominant in the system. To systematically investigate the system's response, we probe the EIS response during the coloring process by gradually increasing the applied potentials and characterize the response through the bleaching process by decreasing the magnitude of the negative potential (Fig. 5). The results for the $LiClO_4$ are provided as a Nyquist plot. The data trends from highest frequency to lowest frequency, from left to right, respectively. When this EIS data is properly plotted on a square-axis format, it is then suitable to analyze the actual shapes of the curves directly per common practice. In the high-frequency region, we observe a clear semi-circle. In the low-frequency region, we

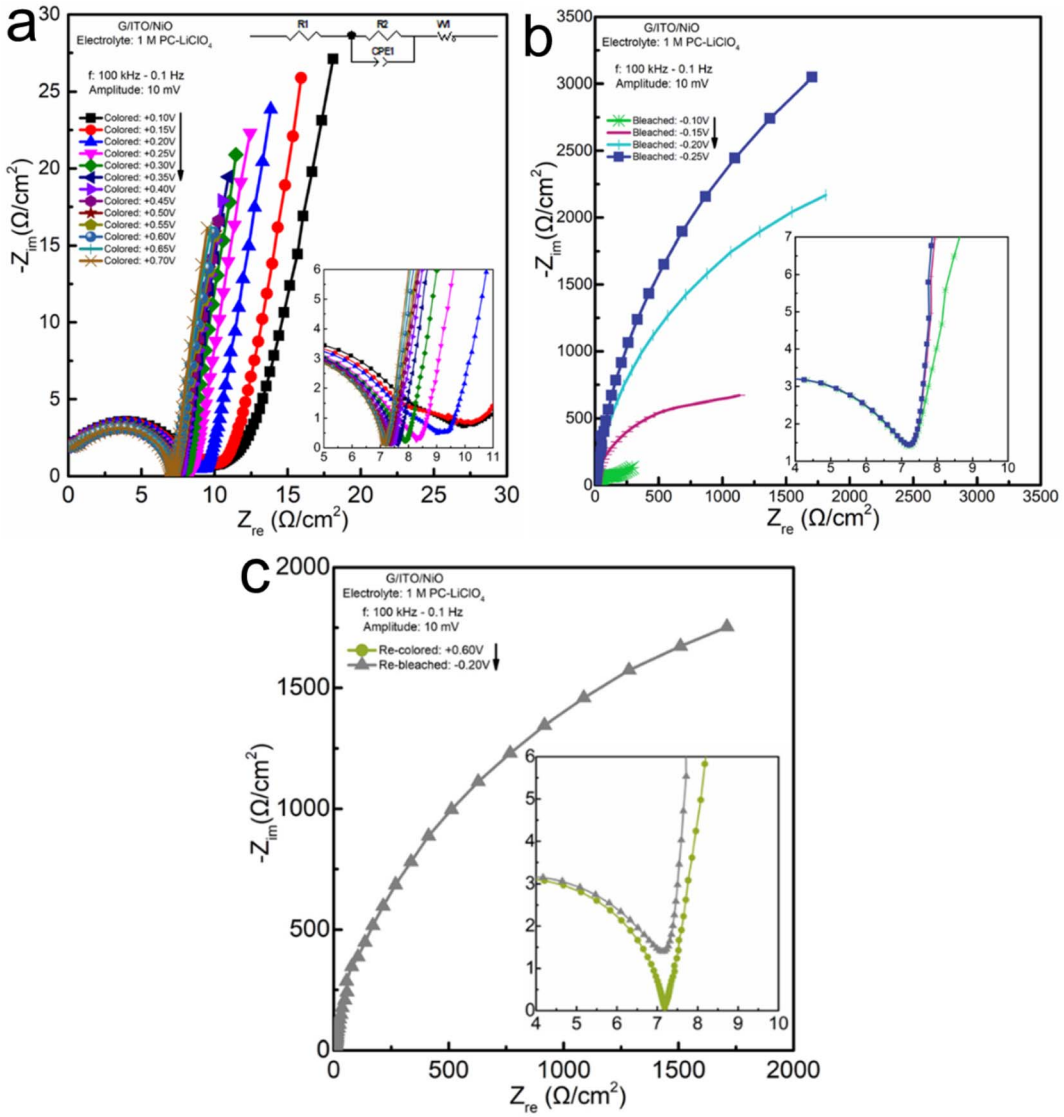

Fig. 5 EIS data and analysis for NiO thin films measured in 1 M PC-$LiClO_4$ electrolyte: (a) Nyquist plot for coloration potentials in the range of (+0.1 V, +0.7 V) with inset fitted equivalent circuit model; (b) Nyquist plot for bleaching potentials in the range of (−0.1 V, −0.25 V); (c) Nyquist of an applied re-coloration potential +0.6 V, and an applied re-bleaching potential −0.2 V. Insets are the proximate high-frequency realm for observation of the transition from the charge transfer resistance into the Warburg region.

observe a linearly increasing complex impedance somewhere at or between 45° (diffusion) and 90° (capacitive) angles.

Nyquist plot PC-LiClO$_4$. By examining the high-frequency region for charge transfer resistance, as shown on the inset of Fig. 5a, we can observe that the diameter of the semicircular region decreases during the coloration process; signifying a decrease in the charge transfer resistance as the external driving force strength is increased. The real impedance Z_{re} decreases from $\cong 10\ \Omega\ cm^{-2}$ down to $\cong 7\ \Omega\ cm^{-2}$, while the imaginary impedance $-Z_{im}$ decreases from $\cong 3.5\ \Omega\ cm^{-2}$ down to $\cong 3\ \Omega\ cm^{-2}$. Comparatively, in Fig. 5b, we do not observe either phenomenon during the bleaching process; instead, for each magnitude increase of the negatively applied potentials, the real and imaginary impedances, being $\cong 7\ \Omega\ cm^{-2}$ and $\cong -1.5\ \Omega\ cm^{-2}$, respectively, remain relatively constant as the different potentials visibly overlap each other. The low-frequency EIS Warburg region will be further scrutinized by the Warburg factor; nevertheless, there are some interesting observations to be made from the Nyquist plots. It is observed that the tail trends closer to the 90° angle through the coloring evolution. What is also noteworthy is that even though the angle of the tail appears to remain unchanged, near the capacitive-denoting 90° angle, it does decrease in magnitude in both the real impedance and the imaginary impedance. Conversely, through the bleaching progression (Fig. 5b), we see a slightly different Warburg tail shape, which does appear to change with the change in external driving force. At the least external potentials (star and horizontal line symbols), we see a clear preference toward the diffusion-denoting 45° angle: however, as the magnitude of the external driving force is increased (vertical line and square symbols), we can see that the tail is inclined between 45° and 90° angles, close to $\cong 60°$ angle for the highest magnitude at the applied potential −0.25 V in bleaching.

In addition to analyzing the lowest-frequency region in the EIS plot, we further analyze the full spectrum of EIS to determine if the overall response of the system is diffusion-controlled, capacitive-dominated, or pseudocapacitive. For example, if we only inspect the lowest frequency-data points the coloration process (Fig. 5a) shows an obvious linear progression of the data in the 90° angle direction. If we again, only look at the lowest frequency data in the bleaching process (Fig. 5b) it appears to be only in the 60° angle direction. However, as you can see clearly in the inset the process starts out towards the 90° angle direction (capacitive) and gradually shifts to the 60° angle direction (diffusion) as the frequency decreases.

Concluding the sequence of EIS investigations for the Li^+ electrolyte, we look into a single re-colored and a single re-bleached potential shown in Fig. 5c. It gives insight into three facets: first, the response in a repeated aspect; second, the response of the instantly applied extreme potential, rather than the gradual progressions: and third a side-by-side comparison of the color *vs.* bleaching complex impedance responses. Comparing the colored at +0.6 V (Fig. 5a) with the re-colored at +0.6 V (Fig. 5c), we can see that the impedance on the right of the semi-circle denoting the end of the charge transfer resistance intercepts the *x*-axis at $Z_{re} \cong 7\ \Omega\ cm^{-2}$ for both the color and re-color data plots. Additionally, the colored and re-colored tails are inclined towards the same angle at the figure insets. Ultimately, there appears to be no significant difference in the impedance responses of the system when the voltage is gradually increased to the highest value *vs.* an instantaneously applied potential. There appears to be no significant difference between the initially colored and re-colored films showing a reliable impedance response. These conclusions also hold for the charge transfer resistance region of the initially bleached and re-bleached. There also appears to be no significant difference comparing the semi-circle of the gradual bleaching to the directly bleached process; nor a significant difference between charge transfer resistance for the initially bleached and re-bleached, showing stability in this regime. We can also observe the pseudocapacitive behavior for direct bleaching compared with the gradual bleaching, although the imaginary

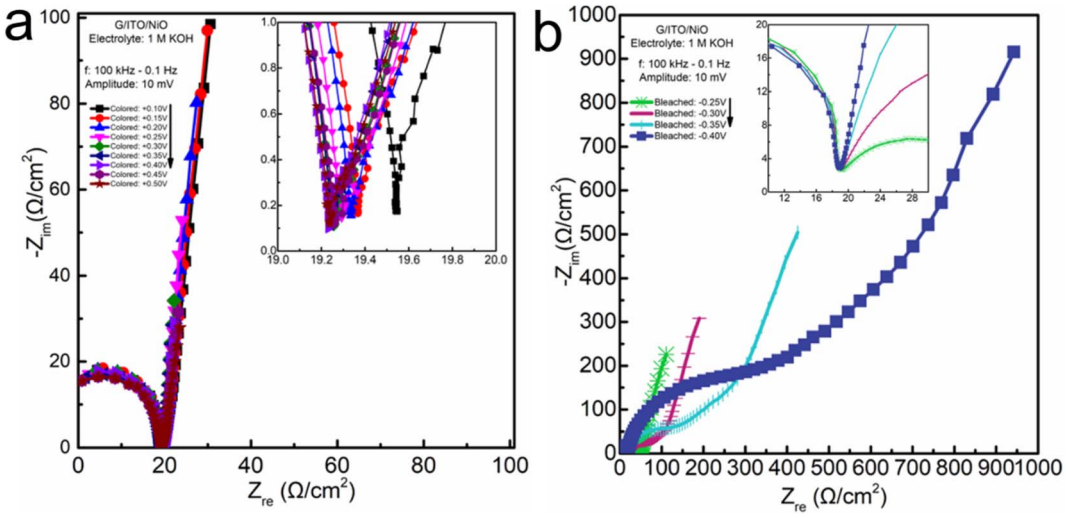

Fig. 6 EIS data and analysis for NiO thin films measured in 1 M KOH electrolyte: (a) gradual coloration applying increased magnitude potentials (+0.1 V, +0.5 V); (b) gradual bleaching range from (−0.25 V, −0.4 V).

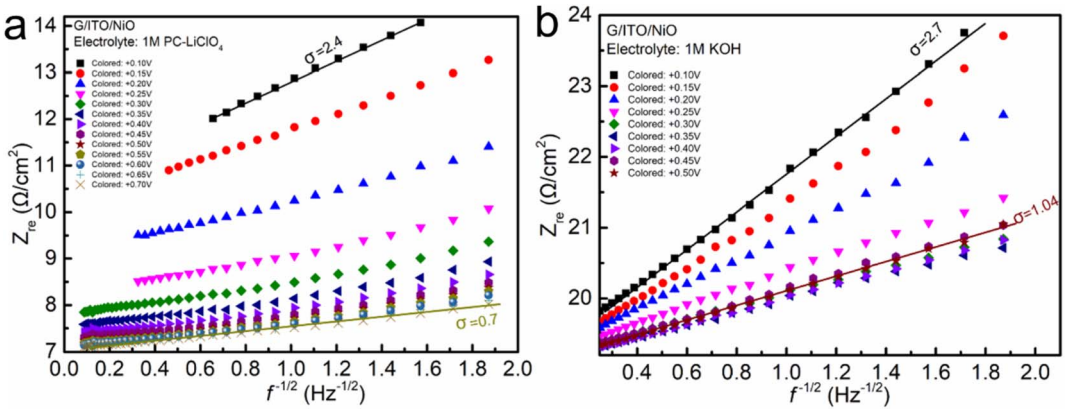

Fig. 7 Warburg factor based on the linear fits of Z_{re} against $f^{-1/2}$ of NiO in non-aqueous Li^+-based and aqueous KOH electrolytes.

impedance does appear to be slightly lower in the direct bleaching Warburg tail, which indicates a slight decrease in the capacitive reactance that occurs in the gradually applied potential process. This could be due to the residual charge in the film occurring during the gradual bleaching process.

Nyquist plot KOH. Significant information to be extracted from the Nyquist EIS data will provide deep insight, and the non-aqueous PC-$LiClO_4$ data will be compared to the aqueous KOH electrolyte EIS. Through the coloring progression in Fig. 6, the complex impedance for the same electrode NiO is

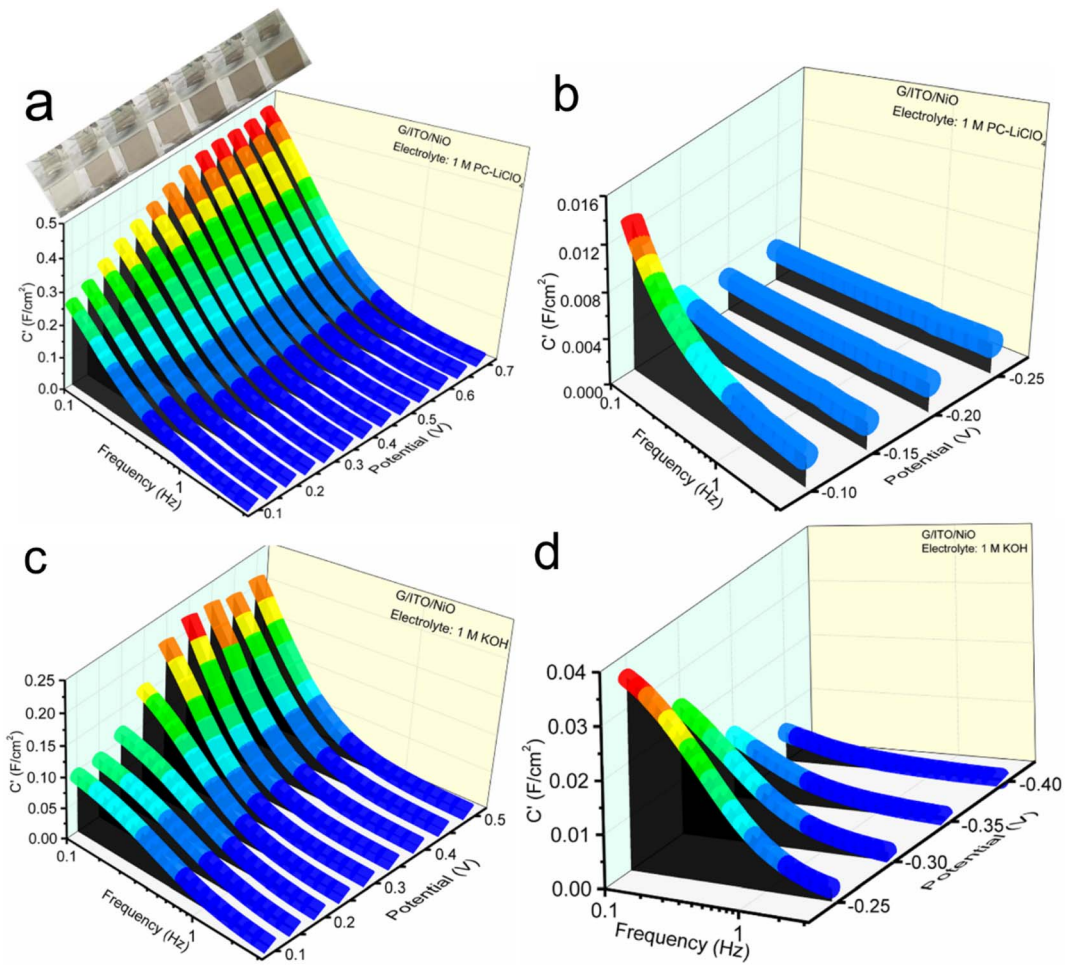

Fig. 8 The 3D Bode plot representations of the real capacitance C' *vs.* f *vs.* potential at firstly charging and then discharging states of NiO in (a and b) PC-Li^+ and (c and d) KOH electrolytes with potentials ranging from 0 up to 0.7 V.

Table 1 Material properties of electrolyte

Properties	Non-aqueous PC-$LiClO_4$	Aqueous KOH
Molar mass	$LiClO_4$ = 106.39 g mol^{-1}	KOH = 56.11 g mol^{-1}
Electron affinity	EA (ClO_4) = 5.25 eV	EA(K) 0.50163 eV
Ionization energy	IE (L) = 5.3917 eV	IE (OH) 13.017 eV
Bandgap	5.74 eV	3.64 eV
Energy above Hull	0.000 eV per atom	0.002 eV per atom
Density	2.42 g mL^{-1}	1.05 g mL^{-1}
Viscosity of solvent (cps)	PC = 2.4	H_2O = 1

significantly higher for the KOH electrolyte compared to the complex impedance of the non-aqueous PC-$LiClO_4$ where the real impedance Z_{re} is $\cong$20 Ω cm^{-2} and $\cong$7 Ω cm^{-2} respectively and the imaginary impedance $-Z_{im}$ is $\cong$100 Ω cm^{-2} and $\cong$25 Ω cm^{-2} for KOH and PC-$LiClO_4$ respectively.

Interestingly, despite demonstrating such a higher complex impedance, the decrease in charge transfer resistance in the KOH electrolyte was less than a 0.4 Ω cm^{-2} shift from $\cong$19.6 down to $\cong$19.2 Ω cm^{-2}. Yet, for the same potentials (+0.1 and +0.5 V) in the PC-$LiClO_4$ with significantly lower overall complex impedance, the decrease in charge transfer resistance was much higher, around 3 Ω cm^{-2} shift from $\cong$10.5 down to $\cong$7.5 Ω cm^{-2}. The similarity between the KOH and PC-$LiClO_4$ is that the Warburg tail is more capacitive, inclining in the capacitive-denoting 90° angle direction through the coloration process. The coloration process occurs during the removal of electrons and Li^+ from the NiO film. De-insertion of Li^+ from thin films tends to consistently reflect capacitive behavior. The more interesting aspects of the impedance are in the bleaching of the NiO film corresponding to the insertion of electrons and Li^+ into the NiO thin films. The bleaching process of the KOH demonstrates a much stronger preference for a diffusion-controlled response as the frequencies that make up the Warburg tail gravitate more strongly toward the diffusion-denoting 45° angle (*i.e.*, frequency to frequency comparison) to the overall response of the PC-$LiClO_4$ Warburg tail region. To reiterate, EIS analysis cannot be limited to the single lowest frequency of the EIS response to determining the angle inclination reflecting diffusion, capacitive, or pseudocapacitive dominated responses, but rather take into consideration the entire spectrum making up the Warburg tail.

Warburg factor. Further investigation for all data points in the Warburg low *f* region can be explored through the plot in Fig. 7 where the fitted slopes are positively proportional to the Warburg coefficient. Warburg coefficients provide insight into ion diffusion in the electrolyte. The Warburg factor, σ, is inversely proportional to the diffusion coefficient of the electrolyte ions, and it has a linear relationship with Z', where $Z' = R_e + R_{ct} + \sigma(2\pi f)^{-1/2}$.[29,30] Here, R_e and R_{ct} are the equivalent resistance and the charge transfer resistance. Fig. 7b you can observe the Warburg coefficient as the slope of the lines in each different electrolyte. The steeper the slope means better diffusion in the system.[31] Comparing the lowest applied voltage +0.1 V you can see that the slope of the PC-$LiClO_4$ is 2.4 and for the KOH is 2.7. The Li-ClO_4 quickly flattens out the more coloration voltage is applied, but the KOH maintains a comparably steeper slope. This shows that KOH has better diffusion for a NiO system. The voltages are applied sequentially from lowest to highest. The more the film is colored the more the film charge storage becomes saturated, thus explaining why the diffusion coefficient decreases with the gradually increasing applied potential. This is further supported by the small diameter of the semi-circular region of the Impedance plots of Fig. 5 and 6 and the *b* values of the log plots in Fig. 3 as previously discussed.

3D Bode plot. The 3D Bode plot (Fig. 8) incorporating capacitance, frequency, and potential allows us to probe further the charge storage/release dynamics associated with the Li^+ insertion/de-insertion and compare at different driving potentials. The lower frequencies provide higher capacitance by allowing the maximum Li^+ insertion/de-insertion to occur in the redox process. This phenomenon occurs in both PC-$LiClO_4$ non-aqueous and aqueous KOH electrolytes. Comparing the electrolytes in the coloration process, we can see that the PC-$LiClO_4$ electrolyte reaches almost twice the maximum capacitance C' ($\cong$0.45 F cm^{-2}) compared to the KOH ($\cong$0.23 F cm^{-2}). The electrical double layer can be indicated through the square-like waterfall shape of the 3D plot, while the capacitance increase with potential reflects the ion-diffusion controlled process.[32] For $LiClO_4$, the capacitance nearly immediately falls off with the bleaching potential at $-$0.15 V even at low frequency. In the KOH, the low-frequency capacitance gradually decreases through the applied potentials and doesn't fully deplete as the PC-$LiClO_4$, even with the applied potential of $-$0.4 V. The slower charge release is due to the ion-diffusion controlled process.

To obtain enhanced capacity, fast response, and improved electrochemical attributes, the inherent properties of the system, *i.e.*, molar mass, electron affinity, ionization energy, electronegativity, viscosity, *etc.*, have been taken into consideration, and the two electrolytes have been compared comprehensively (Tables 1 and 2). The chemical nature of the electrolytes shows a profound effect on electrochemical kinetics of EC NiO films. Based on the tradeoffs in this work, lower electron affinity, ionization energy, and viscosity are likely to be favorable for the ion diffusion and insertion into the NiO electrode.

What is unexpected and quite interesting is that the aqueous KOH showing higher capacity and ion-insertion (bulk) behavior is found to have a higher charge transfer resistance than the Li-PC. This is interesting and unusual; we generally expect that a lower charge transfer resistance is accompanied by a higher

Table 2 Comparison of ion-insertion into NiO comparing non-aqueous *vs.* aqueous electrolyte

Characterizations & analysis	Non-aqueous PC-$LiClO_4$	Aqueous KOH
Charge transfer resistance (EIS)	Low	High
Capacity (CV)	Low	High
Driving potential for 2 mA cm^{-2} (MSCA)	1.0 V	0.2 V
Linear fitting of $\log i_P$ *vs.* $\log \nu$ (CV)	$b = 0.68$ (pseudocapacitive)	$b = 0.56$ (diffusion)
Warburg region (EIS)	$\cong 60° \angle$ (pseudocapacitive)	$\cong 45° \angle$ (diffusion)

charge storage capacity. For example, Nara *et al.* Shows a systematic comparison of capacity *vs.* EIS in lithium batteries. Consistently when you see a decrease in R_{ct} there is a corresponding increase in capacity.[33] Again, in a study conducted by Hang *et al.* we see as the capacity decreases so the charge transfer resistance increases.[34] However, in this study we see the charge transfer resistance for KOH is nearly 20 ohms and the PC-$LiClO_4$ is only 7 ohms. So, we would expect the KOH to have less capacity compared to the PC-$LiClO_4$ but this is not the case. This abnormally points to that the lower charge transfer resistance is not necessarily correlated with higher charge storage capacity when we compare the surface-capacitive dominant and ion-diffusion controlled processes. The coupling effect of the functional cations/anions in electrolyte and electrode materials is not negligible to accomplish enhanced fast charge storage for most sustainable electrochemical energy systems.

Pseudocapacitive charge storage calculation. To quantitively examine the charge storage dynamics, the total current at each potential can be expressed as two processes: the surface capacitive and diffusion-controlled parts: $i(V) = k_1\nu + k_2\nu^{1/2}$ or $i(V)/\nu^{1/2} = k_1\nu^{1/2} + k_2$. By determining k_1 and k_2, we can obtain the current fraction at each potential and then calculate their contributions to the total charge storage. The linear relationship of $i(V)/\nu^{1/2}$ *vs.* $\nu^{1/2}$ enables us to obtain the k_1 and k_2 from the slope and the *y*-axis intercept, respectively, at every single potential.[32] Firstly presented are the classical CV curves between 20 mV s^{-1} and 150 mV s^{-1} scan rates with NiO in Li-PC electrolyte as the demonstration model (Fig. 9a). Subsequently, the 30 mV s^{-1} scan rate is then used to demonstrate the

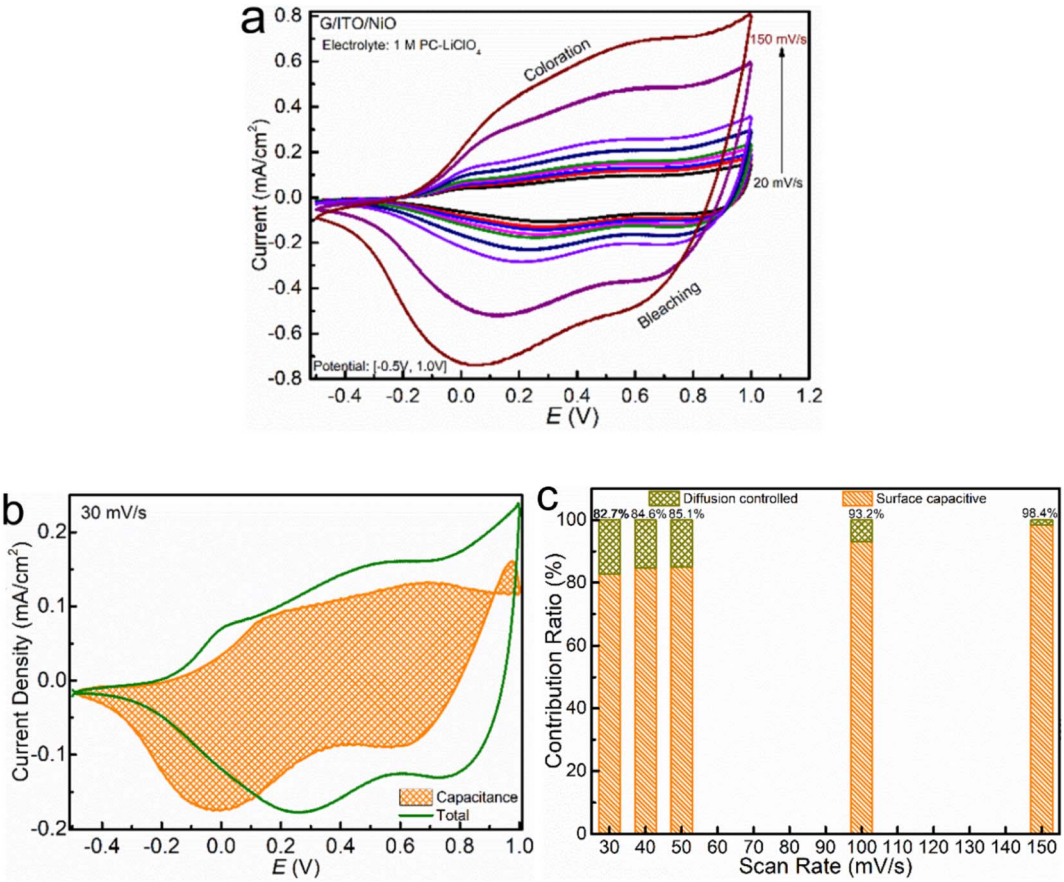

Fig. 9 (a) CV curves from 20 mV s^{-1} to 150 mV s^{-1} scan rates (b) CV curves at 30 mV s^{-1} illustrating the surface capacitance contribution (shadowed area) to the total. (c) Percentage of diffusion-controlled and surface capacitive behavior varying with scan rate.

quantitative analysis shown in Fig. 9b where the shaded area corresponds to the surface capacitive dominant charge storage. The contributions of the ion diffusion-controlled and surface-capacitive response for the NiO thin Films in the Li^+ electrolyte is plotted in the bar plot in Fig. 9c to summarize. Evidently, even at the lowest scan rates, the surface-capacitive mechanism is dominant over the diffusion kinetics for NiO in the 1 M PC-$LiClO_4$ electrolyte, overall presenting a pseudocapacitive system response.

Conclusion

In this exhaustive investigation, we demonstrate electrolyte plays a critical role in the EC NiO charge storage electrochemical system. The working mechanism of different electrolytes toward NiO electrodes is also different, which largely determined the electrochemical behaviors. The electrochemical kinetics and charge transfer in two electrolyte solutions are compared: aqueous KOH and non-aqueous PC-$LiClO_4$, which are evaluated for their effect on the electrochemical response of NiO thin films. The techniques implemented for this comprehensive analysis include CV, MSCA, and EIS techniques. It is found that the PC-$LiClO_4$ electrolyte provides capacitive dominant traits in NiO, while the KOH electrolyte presents battery-dominant performance. Despite the constant working electrode and all other parameters being maintained, the aqueous KOH electrolyte exhibits much higher current densities and capacities with less driving potential and faster response, resulting from the ion-diffusion *versus* surface capacitive controlled kinetics. The mechanism for the electrochromism of NiO and how the interface kinetics are very different in anions (OH^-) and cations (Li^+) based electrolytes have been compared in KOH *vs.* PC-$LiClO_4$. The interaction of NiO electrode and functional ions from electrolytes at interface mainly determines the charge transfer kinetics and electro-optical performance in the system. Several inherent tradeoffs have been considered in the electrolyte, including electron affinity, electron negativity, viscosity, *etc.* The coupling effect of the electrolyte and electrode materials is a key factor for the charge-storage mechanism and EC properties. Further investigation is recommended for accomplishing extraordinary electrochemical performance for EC devices and most other sustainable energy systems.

Experimental

Deposition of NiO thin films

The reactive direct current magnetron sputtering deposition method was implemented as the NiO thin solid film fabrication process. Essential for the thin film deposition is the round Ni target (purity: 99.99%, diameter: 50.08 mm, thickness: 6.35 mm) and a gaseous atmosphere consisting of Ar (purity: 99.99%) and O_2 (purity: 99.99%) at a ratio of 5 : 4 respectively. The pressure at deposition was 3.5 Pa. Power was set at 200 W, and the substrate for deposition was a commercialized transparent conductive indium tin oxide (ITO, square resistance R_s: 30 ohms, thickness: 100 nm) on glass. After deposition, the NiO film thickness was measured by the optical profilometer to be $\cong$350 nm.

Preparation of the electrolyte

The lithium perchlorate ($LiClO_4$) powder (purity: 99+%, Thermo Scientific) and propylene carbonate (PC) liquid (purity: 99.5%, Thermo Scientific) were mixed and stirred for one hour and a half in ambient conditions to get a uniform, a transparent solution with one molar per liter concentration, namely, 1 M PC-$LiClO_4$. The potassium hydroxide (KOH) powder (purity: 99+%, Thermo Scientific) and diluted water were mixed and stirred for one hour and a half in ambient conditions to obtain a uniform, transparent solution with one molar per liter concentration, namely, 1 M KOH.

Characterizations

Structural characterizations were conducted for NiO thin films at each states: initial, bleached, and colored *via* the X-ray Diffractometer (Siemens Model: D 5000), which has an accuracy of $\pm$005° and reproducibility of $\pm$0.0005°. Surface imaging for step height thickness analysis was captured using the state-of-the-art three-dimensional optical profilometer (model: Profilm3D). To ensure a reliable image, the profilometer is stationed on a vibration-resistant table to circumvent the naturally occurring vibrations in the environment. The raw data is processed using the compatible "ProfilmOnline" software. The optical properties of the thin films were determined by using an ultraviolet-visible spectrophotometer (Thermo Scientific, Evolution 220) which features a larger rectangle with a 2 nm spectral bandwidth for enhanced photometric performance. All transmittance values in this work are referred to as the ITO-coated glass substrate at 100% transmittance.

Electrochemical measurements

The electrochemical potentiostat/galvanostat (Metrohm, PGSTAT30 potentiostat) was the apparatus used to obtain the electrochemical data; cyclic voltammetry (CV), multi-step chronoamperometry (MSCA), and electrochemical impedance spectroscopy (EIS). This electrochemical station has a Potential accuracy of $\pm$0.2% SCAN250, a Potential resolution of 0.3 μV ADC10M, Current accuracy of $\pm$0.2% MUX and a Current resolution of 0.00039% (of current range) FI20. Zview software was used for EIS modeling. The experiments were all carried out as a three-electrode system: the working electrode being the NiO-ITO-glass fabricated as described above. The counter and reference electrodes were the platinum (Pt) wire and silver/silver chloride (Ag/AgCl), respectively. The results of the potentials documented in this work are hereby referenced against the Ag/AgCl. As described above, the experiments were designed to characterize and compare the two different electrolytes, 1 M PC-$LiClO_4$, against 1 M KOH. Electrochemical characterizations start at smaller potential windows and increase until NiO's CV redox peaks are complete. Once the potential window was optimized, the NiO electrode with multiple scan rates was also investigated. Due to this EC film's fast response time, the CV

experiments' parameters were run at relatively fast potential scan rates between (200 to 20 mV s^{-1}).

Conflicts of interest

The authors declare no conflict of interest.

Acknowledgements

DOE-M2FCT supports this work under AWD000000013872 (LBNL No. 7621351). DOE-NNSA also supports this work funded under the minority-serving institutional partnership program (MSIPP) ASTERIX consortium under Award NA0003981.

References

1 M. A. Macêdo, L. H. Dall'Antonia, B. Valla and M. A. Aegerter, *J. Non-Cryst. Solids*, 1992, **147–148**, 792–798, DOI: **10.1016/S0022-3093(05)80718-5**.
2 F. G. K. Baucke, *Sol. Energy Mater.*, 1987, **16**(1–3), 67–77, DOI: **10.1016/0165-1633(87)90009-8**.
3 P. Yang, P. Sun and W. Mai, *Mater. Today*, 2016, **19**(7), 394–402, DOI: **10.1016/j.mattod.2015.11.007**.
4 Rare Earth Elements Critical Resources for High Technology|USGS Fact Sheet 087-02, **https://pubs.usgs.gov/fs/2002/fs087-02/**.
5 **https://www.dailymetalprice.com/metalprices.php**.
6 R. Wen, G. A. Niklasson and C. G. Granqvist, *Sol. Energy Mater. Sol. Cells*, 2014, **120**, 151–156, DOI: **10.1016/j.solmat.2013.08.035**.
7 C. Dhas, R. Venkatesh, R. Sivakumar, A. M. E Raj and C. Sanjeeviraja, *Ionics*, 2016, **22**, 1911–1926, DOI: **10.1007/s11581-016-1707-0**.
8 L. Liu, T. Wang, Z. He, Y. Yi, M. Wang, Z. Luo, Q. Liu, J. Huang, X. Zhong, K. Du and X. Diao, *Chem. Eng. J.*, 2021, **414**, 128892.
9 K. S. Kumar, D. Pandey and J. Thomas, *ACS Energy Lett.*, 2021, **6**, 3590–3599.
10 Y. Abe, *et al.*, *Jpn. J. Appl. Phys.*, 2006, **45**, 7780.
11 Q. Zhang, Q. Liu, J. Kang, Q. Huang, Z. Liu, X. Diao and J. Zhai, *Adv. Sci.*, 2018, **5**, 1800163.
12 J. Wang, X. Huo, M. Guo and M. Zhang, *J. Energy Storage*, 2022, **47**, 103597, DOI: **10.1016/j.est.2021.103597**.
13 S. K. Deb, *Appl. Opt.*, 1969, **8**, 192–195.
14 M. H. Chua, T. Tang, K. H. Ong, W. T. Neo and J. W. Xu, *Electrochromic Smart Materials: Fabrication and Applications*, 2019, pp. 1–21.
15 Y. Ding, W. Mengying, Z. Mei and X. Diao, *Sol. Energy Mater. Sol. Cells*, 2022, **248**, 112037, DOI: **10.1016/j.solmat.2022.112037**.
16 F.-Q. Liu, W.-P. Wang, Y.-X. Yin, S.-F. Zhang, J.-L. Shi, L. Wang, X.-D. Zhang, Y. Zheng, J.-J. Zhou, L. Li and Y.-G. Guo, *Sci. Adv.*, 2018, **4**(10), eaat5383, DOI: **10.1126/sciadv.aat5383**.
17 H. P. Chen, J. W. Fergus and B. Z. Jang, *J. Electrochem. Soc.*, 2000, **147**, 399.
18 A. Stenman, *Electrochromic properties of nickel oxide in different electrolytes*, 2013.
19 X. Che, J. Guo, M. Wang, M. Wang, X. Zhong, Q. Liu, G. Dong, X. Wang, J. Yang and X. Diao, *Energy Technol.*, 2021, **9**(12), 2100656, DOI: **10.1002/ente.202100656**.
20 R. Wen, G. A. Niklasson and C. G. Granqvist, *Thin Solid Films*, 2014, **565**, 128–135, DOI: **10.1016/j.tsf.2014.07.004**.
21 K. Xu, *Chem. Rev.*, 2004, **104**, 4303–4418.
22 R. Younesi, G. M. Veith, P. Johansson, K. Edström and T. Vegge, *Energy Environ. Sci.*, 2015, **8**, 1905–1922.
23 S. Passerini, B. Scrosati and A. Gorenstein, *J. Electrochem. Soc.*, 1990, **137**, 3297.
24 R. T. Wen, G. A. Niklasson and C. G. Granqvist, *Thin Solid Films*, 2014, **565**, 128–135.
25 Z. Luo, L. Liu, X. Yang, X. Luo, P. Bi, Z. Fu, A. Pang, W. Li and Y. Yi, *ACS Appl. Mater. Interfaces*, 2020, **12**, 39098–39107.
26 Z. Wu, S. M. Bak, Z. Shadike, S. Yu, E. Hu, X. Xing, Y. Du, X. Q. Yang, H. Liu and P. Liu, *ACS Appl. Mater. Interfaces*, 2021, **13**, 31733–31740.
27 H. Shao, Z. Lin, K. Xu, P. Taberna and P. Simon, *Energy Storage Mater.*, 2019, **18**, 456–461, DOI: **10.1016/j.ensm.2018.12.017ff.ffhal-02359535f**.
28 O. Klymenko, R. Evans, C. Hardacre, I. Svir and R. Compton, *J. Electroanal. Chem.*, 2004, **571**, 211–221, DOI: **10.1016/j.jelechem.2004.05.012**.
29 W. Liu, H. Yi, Q. Zheng, X. Li and H. Zhang, *J. Mater. Chem. A*, 2017, **5**, 10928.
30 K. Li, X. Wang, X. Wang, M. Liang, V. Nicolosi, Y. Xu and Y. Gogotsi, *Nano Energy*, 2020, **75**, 104971.
31 Y. S. Lee and K. S. Ryu, *Sci. Rep.*, 2017, **7**, 16617, DOI: **10.1038/s41598-017-16711-9**.
32 D. Dong, T. E. Benhaddouch, C. L. Metler, J. Marcial, Y. Zhao, V. Venkadesh, T. Thundat and S. Bhansali, *J. Electrochem. Soc.*, 2022, **169**(8), 080511, DOI: **10.1149/1945-7111/ac86a5**.
33 H. Nara, D. Mukoyama, R. Shimizu, T. Momma and T. Osaka, *J. Power Sources*, 2019, **409**, 139–147, DOI: **10.1016/j.jpowsour.2018.09.014**.
34 T. Hang, D. Mukoyama, H. Nara, N. Takami, T. Momma and T. Osaka, *J. Power Sources*, 2013, **222**, 442–447, DOI: **10.1016/j.jpowsour.2012.09.010**.